

Northumbria Research Link

Citation: Garrett, Ed, Shennan, Ian, Woodroffe, Sarah, Cisternas, M., Hocking, Emma and Gulliver, P. (2015) Reconstructing paleoseismic deformation, 2: 1000 years of great earthquakes at Chucalén, south central Chile. Quaternary Science Reviews, 113. pp. 112-122. ISSN 0277-3791

Published by: Elsevier

URL: <https://doi.org/10.1016/j.quascirev.2014.10.010>
<<https://doi.org/10.1016/j.quascirev.2014.10.010>>

This version was downloaded from Northumbria Research Link:
<http://nrl.northumbria.ac.uk/id/eprint/21728/>

Northumbria University has developed Northumbria Research Link (NRL) to enable users to access the University's research output. Copyright © and moral rights for items on NRL are retained by the individual author(s) and/or other copyright owners. Single copies of full items can be reproduced, displayed or performed, and given to third parties in any format or medium for personal research or study, educational, or not-for-profit purposes without prior permission or charge, provided the authors, title and full bibliographic details are given, as well as a hyperlink and/or URL to the original metadata page. The content must not be changed in any way. Full items must not be sold commercially in any format or medium without formal permission of the copyright holder. The full policy is available online: <http://nrl.northumbria.ac.uk/policies.html>

This document may differ from the final, published version of the research and has been made available online in accordance with publisher policies. To read and/or cite from the published version of the research, please visit the publisher's website (a subscription may be required.)

**Reconstructing paleoseismic deformation, 2: 1000 years of great earthquakes at Chucalén,
south central Chile**

E. Garrett ^{a,*}, I. Shennan^a, S.A. Woodroffe^a, M. Cisternas^b, E. P. Hocking^c, and P. Gulliver^d

^a Durham University, Sea Level Research Unit, Department of Geography, South Road,
Durham, DH1 3LE, UK

^b Escuela de Ciencias del Mar, Pontificia Universidad Católica de Valparaíso, Altamirano
1480, Valparaíso, Chile

^c Northumbria University, Department of Geography, Ellison Place, Newcastle upon Tyne,
NE1 8ST, UK

^d NERC Radiocarbon Facility, SUERC, Rankine Avenue, Scottish Enterprise Technology Park,
East Kilbride, G75 0QF, UK

*Corresponding author. Now at The Geological Survey of Belgium, Royal Belgian Institute for
Natural Sciences, Jennerstraat 13, 1000 Brussels, Belgium. Email:
egarrett@naturalsciences.be

Abstract

In this paper we adopt a quantitative biostratigraphic approach to establish a 1000-year-long
coastal record of megathrust earthquake and tsunami occurrence in south central Chile. Our
investigations focus on a site in the centre of the rupture segment of the largest
instrumentally recorded earthquake, the AD 1960 magnitude 9.5 Chile earthquake. At
Chucalén coseismic subsidence in 1960 is recorded in the lithostratigraphy and
biostratigraphy of coastal marshes, with peat overlain by minerogenic sediment and changes
in the assemblages of diatoms (unicellular algae) indicating an abrupt increase in relative sea

level. In addition to the 1960 earthquake, the stratigraphy at Chucalén records three earlier earthquakes, the historically documented earthquake of 1575 and two prehistoric earthquakes, radiocarbon dated to AD 1270 – 1450 and 1070 – 1220. Laterally extensive sand sheets containing marine or brackish diatom assemblages suggest tsunami deposition associated with at least two of the three pre-1960 earthquakes. The record presented here suggests a longer earthquake recurrence interval, averaging 270 years, than the historical recurrence interval, which averages 128 years. The lack of geologic evidence at Chucalén of two historically documented earthquakes, in 1737 and 1837, supports the previously suggested hypothesis of variability in historical earthquake characteristics. Our estimates of coseismic land-level change for the four earthquakes range from meter-scale subsidence to no subsidence or slight uplift, suggesting earthquakes completing each ~270 year cycle may not share a common, characteristic slip distribution. The presence of buried soils at elevations below their modern equivalents implies net relative sea-level rise over the course of the Chucalén paleoseismic record, in contrast to relative sea-level fall over preceding millennia inferred from sites on the mainland. Sea-level rise may contribute to the preservation of evidence for multiple earthquakes during the last millennium, while net relative sea-level fall over the last 2000 to 5000 years may explain the lack of evidence for older earthquakes.

Keywords: Paleoseismicity, earthquake reconstruction, tsunami, relative sea level, diatoms, transfer functions

1. Introduction

Geological approaches to understanding the chronology and characteristics of past earthquakes are essential for assessing potential future hazards posed by subduction zones

(Stein and Okal, 2011). Reliance on short historical records may prevent adequate appreciation of the complexities of subduction zone behaviour, including the occurrence of segmentation, variability in rupture magnitudes and the existence of supercycles (Cisternas *et al.*, 2005; Jankaew *et al.*, 2008; Sieh *et al.*, 2008; Goldfinger *et al.*, 2012; Sawai *et al.*, 2012). In this paper, we adopt a quantitative lithostratigraphic and biostratigraphic approach to reconstruct past earthquakes in south central Chile. The approach, developed in other subduction zone settings (Atwater, 1987; Nelson *et al.*, 1996; Hamilton and Shennan, 2005), is tested along the Chilean coastline in the counterpart to this paper (Garrett *et al.*, 2013). Focusing on a new site at Chucalén, northern Isla de Chiloé (Fig. 1), we aim to: 1) establish whether coastal sediments record evidence for multiple earthquakes and tsunamis; 2) determine the timing of these ruptures; 3) contrast stratigraphic and historical records of earthquakes to assess variability in historical ruptures; 4) calculate the recurrence interval between earthquakes; 5) quantify vertical coseismic deformation for each earthquake and 6) establish whether the record of long-term sea-level change explains the preservation or absence of stratigraphic evidence for earthquakes.

The potential for great earthquakes in south central Chile is well known. The 22nd May 1960 Valdivia, Chile earthquake remains the largest since the inception of modern seismic recording. The earthquake ruptured 1000 km of the Chilean subduction zone between the Arauco Peninsula in the north and the Taitao Peninsula in the south (Fig. 1). Slip on the fault locally reached 40 m, contributing to a moment magnitude (M_w) of 9.5 (Cifuentes, 1989; Barrientos and Ward, 1990). The surface expression of coseismic deformation in 1960 (Fig. 1) featured subsidence up to 2.4 m, coinciding with the coastline, flanked by two regions of uplift (Wright and Mella, 1963; Plafker and Savage, 1970). Uplift of a 100 km wide region offshore locally exceeded 5 m (Plafker and Savage, 1970) and submarine deformation generated a devastating local tsunami, which crested over 20 m high, and a trans-Pacific

tsunami more than 4 m high in Hawaii and Japan (Cox and Mink, 1963; Keys, 1963; Atwater *et al.*, 2005). Along the coast of south central Chile, tidal marsh stratigraphy preserves evidence for the 1960 tsunami in the form of widespread landward-thinning sand sheets abruptly emplaced over intertidal marshes and adjacent organic wetland soils (Wright and Mella, 1963; Cisternas *et al.*, 2000; Bourgeois, 2009; Garrett *et al.*, 2013). Records kept by Spanish settlers and visiting Europeans describe three earlier large earthquakes in south central Chile in 1837, 1737 and 1575 (Lomnitz, 1970); however, the recurrence of earthquakes with 40 m of slip on the fault at approximately 130-year intervals would far exceed the plate convergence rate, implying variability in rupture size, coseismic slip and earthquake magnitude (Stein *et al.*, 1986; Barrientos and Ward, 1990). Stratigraphic evidence for repeated tsunamis accompanied by subsidence in the centre of the 1960 segment supports a longer recurrence interval between 1960-sized earthquakes – approaching 300 years – with partial strain release during smaller intervening ruptures (Cisternas *et al.*, 2005). The 1737 and 1837 earthquakes are inferred to be of shorter rupture length, with reduced slip, however their magnitudes and locations remain unknown (Cisternas *et al.*, 2005; Vita-Finzi, 2011; Moernaut *et al.*, 2014).

2. Study area

The coast of Chile lies above a convergent margin, where the Nazca plate subducts beneath South America at a rate averaging 60 – 80 mm yr⁻¹ (DeMets *et al.*, 1990; Angermann *et al.*, 1999). Strain accumulation results in the occurrence of megathrust earthquakes, great ($M_w > 8$) interplate ruptures that may generate devastating tsunamis. Historical records suggest along-strike segmentation of the subduction zone, with all or part of the 1960 rupture segment also failing in 1837, 1737 and 1575 (Lomnitz, 1970; Barrientos, 2007). Geological evidence for older earthquakes is scarce; Bartsch-Winkler and Schmoll (1993) and

Nelson *et al.* (2009) attribute the fragmentary nature of south central Chilean coastal stratigraphic records to erosion associated with falling late Holocene relative sea level.

In this study, we focus on a new site in the centre of the 1960 segment (Fig. 1). The coastal lowlands and tidal marshes fringing Bahía Quetalmahue, northern Isla de Chiloé, are ideal locations for the preservation of evidence for past relative sea-level change, earthquakes and tsunamis due to the shelter afforded by the Lacui Peninsula to the west and north, the lack of any significant fluvial input and the moderate tidal range (mean higher high water = 1.02m above mean sea level). The site at Chucalén, on the western margin of Bahía Quetalmahue, lies approximately 25 kilometres west of the axis of maximum coseismic subsidence in 1960. Based on the pre- and post-earthquake lower growth limits of terrestrial vegetation, Plafker and Savage (1970) estimate Chucalén subsided coseismically by 1.0 ± 0.2 m in 1960.

3. Materials and methods

3.1 Stratigraphy

The sediment stratigraphy of tidal marshes may record evidence for vertical deformation both during megathrust earthquakes and through the intervening interseismic periods (Atwater, 1987; Nelson *et al.*, 1996). Depending on their position with respect to the locked plate interface, coasts above subduction zones may rise slowly in response to strain accumulation (Fig. 2). Land uplift, experienced at the coast as a gradual fall in relative sea level, is reflected in tidal marsh stratigraphy by a progressive transition from minerogenic to organic sediment deposition. Depending on the location of fault slip with respect to the coastline, subsequent coseismic strain release may cause near-instantaneous land

subsidence (Fig. 2). Experienced at the coast as a rapid rise in relative sea level, subsidence leads to the abrupt emplacement of minerogenic sediments on top of organic marsh soils. The distribution and magnitude of coseismic surface displacement may differ between cycles in response to variation in the location of slip on the fault interface and the amount and heterogeneity of the slip (Wang, 2007).

Sequences of organic intertidal soils interbedded with minerogenic units may reflect cycles of seismic land-level changes (e.g. Atwater, 1987; Darienzo and Peterson, 1990; Shennan *et al.*, 1996; Sawai *et al.*, 2002; Hamilton and Shennan, 2005); however, a range of other sedimentologic, hydrographic, oceanographic and atmospheric processes can give rise to similar stratigraphies (Long and Shennan, 1994; Witter *et al.*, 2001). Following Nelson *et al.* (1996), we attribute organic-minerogenic couplets to coseismic subsidence only where (1) couplets are laterally extensive; (2) organic sediments are buried by sediments indicative of a lower elevation; (3) submergence is sudden and (4) submergence is synchronous at widely spaced sites. The coincidence of submergence with tsunami deposits may also support a coseismic origin (Atwater, 1987; Nelson *et al.*, 1996; Cochran *et al.*, 2005; Sawai *et al.*, 2009), however tsunami deposits are fragmentary and their absence does not negate the association of a sedimentary couplet with an earthquake (Nelson *et al.*, 1996).

Marsh front exposures and a perpendicular transect of 28 closely spaced hand-driven gouge cores reveal the stratigraphy at Chucalén. Box samples taken from an exposure at the seaward end of the coring transect provide sediment samples for laboratory and microfossil analyses and dating.

3.2 Biostratigraphy

Microfossils, particularly diatoms, assist in the identification of tsunami deposits (e.g. Dawson *et al.*, 1996; Hemphill-Haley, 1996) and determination of the amount and suddenness of marsh elevation change (e.g. Shennan *et al.*, 1996; 1999; Sawai *et al.*, 2004). Their utility for quantifying changes in land level stems from the fact that different species occupy different elevations in intertidal environments. While elevation does not directly influence diatom distributions, in coastal marshes it affects flooding frequency and duration, salinity, organic content and grain size; key controls on diatom distributions (Vos and de Wolf, 1993; Gehrels *et al.*, 2001; Patterson *et al.*, 2005). Changes in fossil diatom assemblages, therefore, reflect changes in the elevation of the marsh surface with respect to sea level over time.

We prepare samples for diatom analysis following standard procedures (Palmer and Abbott, 1986), with a minimum of 250 diatom valves counted per sample. We plot assemblage diagrams using C2 software package v.1.7.2 (Juggins, 2011) and provide a visual summary by dividing species into two categories based on their elevation optima in the modern dataset, with dark blue indicating species with optima below mean higher high water (MHHW) and light blue indicating species with optima above MHHW.

We apply transfer function models to estimate the paleommarsh surface elevation associated with each fossil diatom assemblage. These models incorporate contemporary intertidal diatom assemblage data from four marshes in south central Chile, as detailed by Garrett *et al.* (2013). Model selection maximizes the correlation between observed and predicted elevations and minimizes the reconstruction error. The selected transfer function model has a cross-validated r^2 of 0.77 and a root mean square error of prediction of 0.38 m. Assessment of paleommarsh surface elevation reconstructions follow Garrett *et al.* (2013), employing minimum dissimilarity coefficients (MinDC) from the Modern Analogue

Technique in the C2 software package (Juggins, 2011) to measure the similarity between the diatom assemblages in each fossil sample and samples in the modern training set.

The conversion of paleommarsh surface elevation to estimates of relative sea level requires the field elevation of each sample. We define relative sea level relative to present mean sea level as:

$$RSL_n = FE_n - PMSE_n \quad (1)$$

Where:

RSL_n = Relative sea level estimate for sample n

FE_n = Field elevation of sample n (metres, present mean sea level)

$PMSE_n$ = Paleommarsh surface elevation (metres, mean sea level at time of deposition)

Sample specific 95% error terms are the root of the sum of the squared errors in reconstructing the paleommarsh surface elevation and estimating the field elevation of samples. The difference between pre- and post-earthquake RSL estimates defines the magnitude of coseismic deformation.

3.3 Chronology

We base the Chucalén chronology on AMS radiocarbon dating of herbaceous plant macrofossils. Where possible, we select horizontally bedded above ground parts of terrestrial plants, however below ground material may contribute to samples where more favourable material was lacking. We report dates as ^{14}C years BP and calibrate to 2σ age

ranges in years AD using the SHCal13 calibration curve (Hogg *et al.*, 2013). For samples exceeding 100 % modern carbon, we employ the post-bomb atmospheric southern hemisphere ¹⁴C curve (Hua and Barbetti, 2004). Stratigraphic ordering allows these samples to be fitted to either the rising or the falling limb of the post-bomb curve and single calibration solutions to be obtained (supplementary Fig. S1). The age model uses the Bayesian *P_sequence* approach in OxCal 4.2 (Bronk Ramsey, 2009).

4. Results

4.1 Stratigraphy

Marsh front exposures at Chucalén display four abrupt transitions from organic to minerogenic deposition (Fig. 3). We refer to the four buried organic units as Soils A, B, C and D, with A the uppermost and D the lowermost. The buried soils are continuous and largely uninterrupted for more than 300 m in marsh front exposures and a series of 28 hand-drilled cores maps the couplets as they rise across tidal marsh and freshwater meadow (Fig. 3; supplementary figure S2).

Buried soil A is mid to dark brown, sandy and locally contains the remains of woody plants, tree stumps and other herbaceous plant material, including the rhizomes of *Spartina densiflora* and *Juncus balticus*. The overlying one- to ten-centimetre-thick mid grey sand sheet flattens and encases vegetation rooted in Soil A. The sand deposit decreases in thickness with increasing distance from the marsh front and extends more than 75 m inland (Fig. 2). Additional sand lenses more than 100 m inland may be a continuation of this sand sheet, however their discontinuous nature precludes their unequivocal correlation.

Soil B, occurring in marsh front exposures and 17 cores at the seaward end of the coring transect, is mid to dark brown and sandy (Fig. 3). It lacks the rhizomes and woody plant remains found in Soil A, but contains fragments of herbaceous plants and humified organic matter. A light brown to mid grey sand sheet overlies the soil and extends at least 80 m inland from the marsh front. The deposit is generally thicker than the sand sheet overlying Soil A, with a maximum thickness of 18 cm.

Buried soil C is mid to very dark brown and silty, with herbaceous plant remains, but no woody plant material. The overlying light grey-brown silty sand sheet is generally 5 to 10 cm thick, however the precise thickness of the deposit is difficult to ascertain as it grades into the base of Soil B. The contact between Soil C and the minerogenic unit can be traced 80 m inland from the marsh front. The upper part of the buried soil features numerous sub-centimetre burrows filled with the overlying silty sand (Fig. 3; supplementary Fig. S2).

Soil D, the lowermost buried soil, is mid to very dark brown and silty, with occasional herbaceous plant fragments and no woody plant remains. A light brown to mid grey silty sand sheet overlies the soil. At 3 to 5 cm thick, this deposit is generally thinner than the minerogenic units overlying the three other buried soils and does not extend as far inland (Fig. 3).

4.2 Chronology

Twelve AMS radiocarbon samples provide a chronology for the Chucalén sedimentary sequence (Table 1). We exclude four other dates where visual assessment and outlier analysis suggest downward root penetration has resulted in younger ages than their stratigraphic position would suggest. We adjust the depths to exclude three sand layers,

which we interpret as tsunamis (discussed in section 5.1). Bayesian age modelling in OxCal v.4.2 (Bronk Ramsey, 2009) provides an age-depth model (Fig. 4) with an overall agreement index of 69.1, indicating satisfactory agreement between prior and posterior age distributions (Table 1). Calibrated ages indicate the sediments accumulated over the last millennium. The age model constrains the timing of the abrupt upper contact of Soil A to AD 1955 – 1971 (Fig. 4). This supports the mid- to late-20th century age inferred from elevated caesium-137 concentrations (Garrett *et al.*, 2013), and confirms the association of the burial of Soil A with subsidence during the 1960 earthquake. The large range in ages for the burial of Soil B, AD 1540 – 1800, reflects uncertainties introduced by calibrating dates from the sixteenth to nineteenth century radiocarbon plateau. The upper contact of Soils C and D date to AD 1270 – 1450 and AD 1070 – 1220 respectively (Fig. 4).

4.3 Biostratigraphy

Diatom assemblages in samples from the marsh front exposure contain species indicative of intertidal environments (Fig. 5). Of the 143 taxa encountered, 117 occur in the modern training set and 21 exceed 10 % of the total diatom count in one or more sample. Calibration of assemblages using the south central Chile transfer function (Garrett *et al.*, 2013) yields reconstructions of paleomarch surface elevation, which we convert to relative sea-level reconstructions (Fig. 5).

High marsh species dominate diatom assemblages from Soil A. An abrupt change to assemblages containing species with a range of elevation preferences marks the transition to the overlying sand sheet. After an initial peak in one species with a modelled elevation optimum above mean higher high water (MHHW), the base of the modern marsh soil predominantly features species with optimum elevations below MHHW.

286

287 Species typically found below MHHW occur in Soil B, with only occasional taxa from
288 environments higher in the intertidal zone. The overlying sand sheet contains increased
289 percentages of these low elevation species, with abrupt changes only observed in the
290 abundances of minor species. Immediately above the sand sheet, diatoms from the base of
291 Soil A feature increased percentages of species with optimum elevations above MHHW.

292

293 Buried Soil C contains a range of species from high marsh environments, alongside the
294 ubiquitous *Pseudostaurosira perminuta*. An abrupt decrease in the abundances of high
295 marsh species marks the boundary with the overlying silty sand. Species with optimum
296 elevations below MHHW characterise the silty sand and continue to be found in the base of
297 Soil B alongside occasional taxa from higher marsh elevations.

298

299 As found in Soil C, Soil D features high marsh species together with *Pseudostaurosira*
300 *perminuta*. While *P. perminuta* remains abundant in the overlying silty sand, the high marsh
301 species abruptly give way to low elevation taxa. Species characteristic of low intertidal
302 elevations continue to dominate assemblages from the base of Soil C.

303

304 **5. Discussion**

305

306 **5.1 Evidence for multiple earthquakes**

307

308 The stratigraphic, microfossil and radiocarbon results from Chucalén provide evidence for
309 laterally continuous buried soils, submerged by abrupt relative sea-level rise at similar times
310 to episodes of coseismic subsidence and tsunami deposition reported by Cisternas *et al.*
311 (2005) from Maullín. We test the hypothesis that each buried soil at Chucalén records the

occurrence of an earthquake, focusing on the criteria outlined by Nelson *et al.* (1996),
evidence for tsunami deposition and the modelled timing of the burial of each soil.

Soil A

Buried soil A is laterally extensive and diatom assemblages indicate a sudden transition to
sediments deposited at a lower elevation. The transfer function model estimates subsidence
of 0.81 ± 1.04 m, increasing to 1.12 ± 1.03 m if the lowest post-earthquake sea-level
reconstruction, 4 cm above the upper boundary of the sand sheet, is selected (Fig. 5; Table
2). The magnitude of modelled subsidence is in good agreement with the 1.0 ± 0.2 m
documented by Plafker and Savage (1970) for the AD 1960 earthquake.

Based on local testimony, Garrett *et al.* (2013) interpret the sand sheet overlying Soil A as
the deposit left by the 1960 tsunami. While storms, river floods and aeolian processes may
also deposit sand sheets in intertidal settings, the sheltered location of the site and the lack
of nearby rivers or subaerial sand sources support the tsunami interpretation. We do not
attempt to infer the maximum landward extent of the deposit or the tsunami inundation
limit as ploughing and trampling by livestock precludes identification of the deposit at higher
elevations.

Radiocarbon age modelling constrains the timing of the abrupt burial of Soil A to AD 1955 –
1971 (Fig. 4), corroborating the correlation with the 1960 earthquake previously inferred
from ^{137}Cs concentrations (Garrett *et al.*, 2013).

Soil B

The lateral extent and abrupt nature of the upper contact support coseismic subsidence as
the mechanism for the burial of Soil B. The diatom data, however, do not suggest that the

soil is overlain by sediments indicative of a lower elevation. On the contrary, there is a net sea-level fall between the top of Soil B and the bulk of Soil A (Table 2), clearly reflected in the diatom assemblages, although the 95% error terms for the reconstructions and number of poor modern analogues (Fig. 5) point to the need for a larger modern dataset to improve the transfer function models. The diatom assemblages in the basal 1 cm of Soil A are more transitional, but they could either reflect a mix of the assemblages from the sand with those of the new environment developing on an uplifted marsh, or suggest there is no elevation change across the sand, followed by gradual relative sea-level fall.

We interpret the sand layer overlying Soil B as a tsunami deposit. Like the 1960 tsunami deposit, this sand layer is laterally extensive and coarse grained, with well-defined lower and upper contacts. Diatom assemblages indicate a marine rather than fluvial or terrestrial sediment source. The highly enclosed nature of Bahía Quetalmahue does not favour storm surges as a mechanism for the emplacement of decimetre-thick sand sheets at Chucalén.

The timing of burial, AD 1540 – 1800, overlaps with two major historical earthquakes in 1575 and 1737. While other processes cannot yet be completely discounted, we suggest the 1575 earthquake and tsunami provides the most plausible candidate for the stratigraphy at Chucalén. At Maullín, 45 km to the northeast, Cisternas *et al.* (2005) present sedimentary, dendrochronological and documentary evidence for coseismic subsidence and tsunami inundation in 1575. While the 1737 earthquake also falls within the age range of the burial of Soil B at Chucalén, historical records do not mention a tsunami associated with this earthquake (Lomnitz, 1970; Cisternas *et al.*, 2005) and there is no geological evidence for the earthquake or tsunami at Maullín (Cisternas *et al.*, 2005).

We conclude that the simplest explanation for the burial of Soil B and net uplift between the

top of Soil B and the bulk of Soil A is either coseismic uplift or no coseismic elevation change followed by rapid post-seismic uplift. The latter would imply a spatial pattern of coseismic and post-seismic motions similar to that described by Sawai *et al.* (2004) from Japan; and both explanations imply a different pattern of rupture and surface deformation for the 1960 and 1575 earthquakes. We highlight that this reconstruction comes from a single exposure and that local factors such as erosion of the surface of Soil B could impact on the magnitude of deformation recorded.

Soil C

Found throughout the lower half of the coring transect, Soil C is laterally extensive and abruptly overlain by sediments containing diatom assemblages indicative of a lower intertidal elevation (Fig. 5). The estimated magnitude of deformation depends on the interpretation of the minerogenic unit overlying the buried soil. The upper contact of the soil is clearly defined, but in the sampled exposure the presence of burrows filled with the overlying silty sand suggests bioturbation. Cisternas *et al.* (2005) note the similar appearance of a buried soil at Maullín and propose that this reflects post-subsidence erosion and burrowing by intertidal organisms. Abruptly emplaced tsunami sand sheets may mantle soils, preventing bioturbation and maintaining the intact nature of the contact. If no tsunami sediment was deposited on Soil C at this particular location, the minerogenic sediments overlying the soil accumulated after the earthquake and are therefore indicative of the post-earthquake land level. Comparison of diatom assemblages across the contact suggests subsidence of 0.92 ± 1.20 m (Table 2). If the minerogenic unit incorporates reworked tsunami-lain sediment, the diatom assemblages may not reflect the post-earthquake land level. Comparison of samples from Soil C and the base of Soil B suggests subsidence of 0.69 ± 1.17 m.

The age model constrains the timing of the burial of Soil C to AD 1270 – 1450 (Fig. 4). This overlaps the most recent prehistoric earthquake recorded at Maullín, AD 1280 – 1390 (Cisternas *et al.*, 2005), supporting the occurrence of synchronous submergence at different sites.

Soil D

The lowermost buried soil is laterally extensive, found in 14 of the 28 cores and in marsh front exposures, and abruptly overlain by a tabular silty sand deposit. Comparison of diatom assemblages from the top of Soil D and the base of Soil C using the transfer function model suggests abrupt subsidence of 0.60 ± 1.10 m (Fig. 5; Table 2). While the lack of good modern analogues for the assemblages encountered in Soil D again highlights the need for a larger modern dataset, the reconstructed relative sea levels make ecological sense given the distribution of the major species in the modern environment.

As with the minerogenic layers overlying Soils A and B, tsunami deposition is the favoured hypothesis for the emplacement of the silty sand sheet overlying Soil D. The abundant low elevation diatoms found in this unit indicate a marine sediment source (Fig. 5). The lack of evidence for bioturbation of Soil D and a relatively well defined upper contact at the base of Soil C favour tsunami deposition over gradual sediment accumulation on a post-subsidence tidal flat.

The timing of the burial of Soil D, AD 1070 – 1220, closely corresponds to the age range of evidence for subsidence and tsunami inundation at Maullín, AD 1020–1180 (Cisternas *et al.*, 2005).

5.2 Variability in historical earthquake ruptures

416

417 When compared to historical records of earthquakes, coastal sediments at Chucalén appear
418 to underrepresent the frequency of major earthquakes in south central Chile. The absence
419 of evidence for the 1737 and 1837 earthquakes at Chucalén suggests variability in the
420 characteristics of the historical ruptures. Several lines of evidence suggest the 1737 and
421 1837 earthquakes ruptured smaller areas of the plate interface and generated less damaging
422 tsunamis than the earthquakes of 1575 and 1960 (Lomnitz, 1970; Cisternas *et al.*, 2005;
423 Moernaut *et al.*, 2014). The 1737 earthquake produced isolated accounts of damage in
424 Valdivia and Chiloé (Lomnitz, 1970, Cisternas *et al.*, 2005). The lack of any reports of tsunami
425 occurrence may reflect the location of the rupture with respect to populated areas or the
426 faulting mechanism not resulting in a large tsunami. Using a quantitative lacustrine turbidite
427 approach, Moernaut *et al.* (2014) suggest the 1737 earthquake ruptured an area to the
428 north of Chiloé. Like at Maullín (Cisternas *et al.*, 2005), we find no evidence for the 1737
429 earthquake at Chucalén. The lack of deformation implies a different rupture pattern to that
430 associated with the 1960 earthquake and is consistent with the rupture area proposed by
431 Moernaut *et al.* (2014).

432

433 While the 1837 earthquake produced a large trans-Pacific tsunami, records of the tsunami
434 are not as widespread along the Chilean coast as in 1575 and 1960, with no reports of
435 extensive damage (Lomnitz, 1970; Lander and Lockridge, 1989; Atwater *et al.*, 2005).
436 Coseismic uplift in the Chonos Archipelago may suggest a rupture area in the southern half
437 of the 1960 segment (Lomnitz, 1970). While Concepción experienced intense shaking
438 (Cisternas *et al.*, 2005) and the earthquake triggered turbidites in lakes north east of Valdivia
439 (Moernaut *et al.*, 2014) and in Reloncaví Fjord (St-Onge *et al.*, 2012), neither the stratigraphy
440 nor the biostratigraphy at Chucalén shows evidence for tsunami inundation or abrupt
441 changes in relative sea level during this period (Fig. 5). Combined with the lack of evidence

for deformation at Maullín (Cisternas *et al.*, 2005), we suggest the northern extent of the 1837 rupture lies to the south of northern Chiloé or that any slip occurring in this region was minimal. This interpretation is consistent with a rupture length of up to 500 km and does not preclude near-trench strain release as proposed by Moernaut *et al.* (2014).

5.3 Recurrence of great Chilean earthquakes

The paleoseismic record at Chucalén spans a period approximately twice as long as that covered by historical records. While the four historically documented earthquakes in 1960, 1837, 1737 and 1575 have an average recurrence interval of 128 years, the Chucalén record suggests a longer interval, averaging approximately 270 years. Our modelled earthquake ages are consistent with dates for subsidence and tsunami deposition at Maullín (Cisternas *et al.*, 2005; Fig. 6). Furthermore, the timing of earthquakes in the Chucalén record coincides with evidence for intense shaking from turbidites in lakes Villarica, Calafquén and Riñihue, located approximately 300 km to the north (Fig. 6). In these lakes, a varve-counting procedure further constrains the timing of two proposed full-segment ruptures to AD 1319 \pm 9 years and AD 1127 \pm 44 years (Moernaut *et al.*, 2014).

5.4 Implications for earthquake deformation cycles

Evidence from Chucalén, Maullín and lakes north east of Valdivia suggests partial ruptures featuring less coseismic slip in 1737 and 1837 occurred in the interval between full segment ruptures in 1575 and 1960. Moernaut *et al.* (2014) identify evidence for an additional, previously unrecognised earthquake, dated to AD 1466 \pm 4 years. The low seismic intensity inferred from their lacustrine turbidite records and the lack of evidence for deformation or tsunami inundation at coastal sites in the centre of the 1960 rupture area (Cisternas *et al.*,

2005; this study) suggest this earthquake constitutes another partial segment rupture. Cisternas *et al.* (2005) assert that stress held over smaller ruptures contributed to the size of the 1960 earthquake; the identification of an earlier partial rupture suggests this process could also have contributed to the size of pre-1960 full segment earthquakes.

In addition to supporting the occurrence of a bimodal rupture pattern featuring both partial and full segment ruptures, the paleoseismic record from Chucalén also suggests possible variability in the characteristics of the proposed full segment ruptures, reflected by estimates of coseismic deformation (Fig. 5; Table 2). The earthquakes of 1960 and AD 1270 – 1450 appear similar at Chucalén; that of AD 1070 – 1220 produced less subsidence, whereas that of AD 1575 may have entailed no subsidence or even slight uplift. In contrast, historical records of the 1575 earthquake share extensive similarities with the damage, deformation and tsunami inundation observed in 1960 (Lomnitz, 1970; Cisternas *et al.*, 2005). Lacustrine turbidites suggest that the 1575 and 1960 earthquakes featured similar seismic intensities in the northern half of the segment (Moernaut *et al.*, 2014), with marine turbidites from the centre of the 1960 rupture zone also displaying similar thicknesses for the two earthquakes (St-Onge *et al.*, 2012). We stress that our finding of differential deformation is only from a single location at present and could reflect the limitations of the modern dataset or site-specific processes. Further quantitative estimates are needed to confirm or refute the magnitude of deformation inferred by this study. If confirmed, a lack of subsidence in 1575 at Chucalén could indicate a different spatial pattern of slip during this earthquake. We suggest that this could reflect less slip in the vicinity of northern Chiloé, or slip further down-dip, moving the boundary between zones of uplift and subsidence to the east of its position in 1960 (Fig. 1). At present there are too few studies using quantitative reconstructions of surface deformation based on paleoseismic evidence to differentiate between detailed models of rupture dimensions. We have some constraints on the spatial patterns of

deformation, but insufficient detail to estimate the depth of the slip patch or the amount of slip. Research on other subduction zones demonstrates the potential for coastal paleoseismology to constrain rupture parameters (e.g. Sawai *et al.*, 2004, Wang *et al.*, 2013; Shennan *et al.*, 2014) and shows how quantitative paleoseismology in Chile may progress. We also advocate the need for continued and enhanced integration of coastal deformation and tsunami records with earthquake reconstructions from lacustrine and marine turbidites to determine the characteristics of both full and partial segment ruptures in south central Chile.

5.5 Long-term relative sea-level change

Long-term sea-level rise provides accommodation space and promotes sediment accumulation and the preservation of stratigraphic evidence for earthquakes in intertidal environments (Dura *et al.*, 2011; Grand Pre *et al.*, 2012). In this section we assess the evidence for long-term relative sea-level change at Chucalén and discuss the implications for the length of the paleoseismic record at this site.

The occurrence of organic marsh soils at elevations below their contemporary elevation of formation implies relative sea-level rise over the course of the Chucalén record. Figure 7 compares relative sea-level estimates derived from our model estimates and field elevations at Chucalén with published data from the estuary of the Río Maullín on the adjacent mainland (Atwater *et al.*, 1992). Discarding a single point from Maullín located below present sea level due to the likelihood of compaction, as noted by the original authors, we see a clear contrast between the datasets. The relative sea-level rise seen over the last 1000 years at Chucalén is not the dominant mid to late Holocene trend at Maullín, where tidal marsh sediments above their contemporary depositional elevations suggest net relative sea-

level fall over the last 2000 to 5000 years (Atwater *et al.*, 1992). Glacial isostatic adjustment models also suggest falling relative sea level characterized the Pacific coast of South America during the late Holocene (Fig. 7; Peltier, 2004). Falling sea level reduces accommodation space and favours erosion over sediment deposition. Nelson *et al.* (2009) evoke this process for the scarcity of paleoseismic evidence in the Valdivia estuary; falling relative sea level may also explain the lack of evidence for earthquakes older than ~ AD 1100 at Chucalén.

The causes of sea-level rise at Chucalén over the last millennium remain equivocal and could relate to the magnitude of coseismic subsidence exceeding interseismic uplift, regional tectonics, isostatic subsidence due to the collapse of a neoglacial forebulge or eustasy, while site-specific factors including compaction could also contribute. The discrepancy between observations and models of late Holocene Chilean relative sea level is not currently adequately explained and deserves further investigation.

6. Conclusions

Laterally extensive buried soils with abrupt upper contacts and evidence for rapid and substantial marsh surface elevation change suggest sediments at Chucalén record evidence for repeated great earthquakes. The major conclusions of our work are:

1. Predecessors of the 1960 great earthquake occurred in AD 1540 – 1800, 1270 – 1450 and 1070 – 1220. These ages closely correspond with maximum ages for tsunami deposition and submergence at Maullín (Cisternas *et al.*, 2005) and turbidite deposition in lakes north east of Valdivia (Moernaut *et al.*, 2014). We interpret the sequence as including evidence for two historically documented earthquakes and tsunamis, in 1575 and 1960.
2. The lack of evidence for tsunami deposition and land-level change corresponding to

historically documented earthquakes in 1737 and 1837 supports the hypothesis of variability in historical earthquake rupture zones. We suggest the earthquakes absent from the Chucalén stratigraphy had smaller rupture zones to the north or south of northern Chiloé.

3. The Chucalén record underrepresents the frequency of great earthquakes in south central Chile. The recurrence interval between the four earthquakes, approximately 270 years, is more than twice the interval inferred from historical records.
4. Vertical coseismic deformation estimates vary between earthquakes. Diatom assemblages indicate decimetre to metre-scale subsidence at Chucalén in AD 1960 and AD 1270 – 1450, approximately half that in AD 1070 – 1220, and no subsidence or even slight uplift in AD 1575. Earthquakes completing each ~270 year cycle may not share a common, characteristic slip distribution; however, there are currently too few quantitative estimates of deformation to differentiate between detailed models of the distribution, depth or the amount of coseismic slip.
5. In contrast to relative sea-level fall over the last 2000 to 5000 years inferred from sites on the mainland, the presence of stacked sequences of buried soils implies rising relative sea levels over the last 1000 years at Chucalén. A shift from sea-level fall to sea-level rise may explain the preservation of earthquakes during the last millennium and the absence of older evidence.
6. Quantitative paleoseismology based on coastal marshes in Chile is still at an early stage compared to some other subduction zones but the results described here demonstrate the potential of such methods and indicate some ways ahead for future investigations through the development of more extensive modern training sets to quantify land surface deformation at a larger number of coastal sites. This will provide better data to constrain models of segment ruptures, including depth and amount of slip.

572

573 **Acknowledgements**

574 EG thanks the Royal Geographical Society (with the Institute of British Geographers), the
575 British Society for Geomorphology, the Quaternary Research Association and Santander. MC
576 funded by Project FONDECYT N° 1110848. Caroline Taylor, Rob Wesson and Tina Dura
577 provided assistance in the field. Frank Davies, Kathryn Melvin, Neil Tunstall, Martin West,
578 Amanda Hayton and Alison George provided laboratory assistance. Radiocarbon support was
579 provided by the NERC Radiocarbon Facility NRCF010001 (allocation number 1727.1013). We
580 thank Rob Witter and an anonymous reviewer for their constructive comments and
581 suggestions. This paper is a contribution to IGCP project 588 “Preparing for coastal change: A
582 detailed process–response framework for coastal change at different timescales”.

References

- Angermann, D., Klotz, J., Reigber, C., 1999. Space-geodetic estimation of the Nazca-South America Euler vector. *Earth and Planetary Science Letters*, 171, 329-334.
- Atwater, B. F. 1987. Evidence for Great Holocene earthquakes along the outer coast of Washington State. *Science*, 236, 942-944.
- Atwater, B., Jiménez, H., Vita-Finzi, C. 1992. Net late Holocene emergence despite earthquake- induced submergence, South Central Chile. *Quaternary International*, 15/16, 77-85.
- Atwater, B.F., Musumi-Rokkaku, S., Satake, K., Tsuji, Y., Ueda, K., Yamaguchi, D., 2005. *The Orphan Tsunami of 1700*. Virginia, United States Geological Survey.
- Barrientos, S. E. 2007. Earthquakes in Chile. In: MORENO, T., GIBBONS, W. (eds.) *The Geology of Chile*. London: The Geological Society. pp. 263-287.
- Barrientos, S.E., Ward, S.N., 1990. The 1960 Chile Earthquake – inversion for slip distribution from surface deformation. *Geophysical Journal International*, 103, 589-598.
- Bartsch-Winkler, S., Schmoll, H. 1993. Evidence for late Holocene relative sea-level fall from reconnaissance stratigraphical studies in an area of earthquake-subsided intertidal deposits, Isla Chiloé, southern Chile. In: Frostwick, L. E., Steel, R. J. (eds.) *Tectonic controls and signatures in sedimentary successions*. International Association of Seismologists. pp. 91-108.
- Bourgeois, J., 2009. Geologic effects and records of tsunamis. In: Robinson, A.R. and Bernard, E.N., eds., *The Sea, Volume 15: Tsunamis*. Harvard University Press, p. 53-91.
- Bronk Ramsey, C., 2009. Bayesian Analysis of Radiocarbon Dates. *Radiocarbon*, 51, 337-360.
- Cifuentes, I. L., 1989. The 1960 Chilean earthquake. *Journal of Geophysical Research*, 94, 665-680.

608 Cisternas, M., Contreras, I., Araneda, A. 2000., Recognition and characterisation of the
609 sedimentary facies deposited by the 1960 tsunami in the Maullín estuary, Chile. *Revista*
610 *Geologica De Chile*, 27, 3-11.

611 Cisternas, M., Atwater, B. F., Torrejon, F., Sawai, Y., Machuca, G., Lagos, M., Eipert, A.,
612 Youlton, C., Salgado, I., Kamataki, T., Shishikura, M., Rajendran, C. P., Malik, J. K., Rizal, Y.,
613 Husni, M., 2005. Predecessors of the giant 1960 Chile earthquake. *Nature*, 437, 404-407.

614 Cochran, U., Berryman, K.R., Mildenhall, D.C., Hayward, B.W., Southall, K., Hollis, C.J., 2005.
615 Towards a record of Holocene tsunami and storms for Northern Hawke's Bay, New
616 Zealand. *New Zealand Journal of Geology and Geophysics*, 48, 507–515.

617 Cox, D., Mink, J. F., 1963. The Tsunami of 23 May 1960 in the Hawaiian Islands, *Bulletin of*
618 *the Seismological Society of America*, 53, 1191-1209

619 Darienzo, M.E., Peterson, C.D., 1990. Episodic tectonic subsidence of late Holocene salt
620 marshes, Northern Oregon coast, central Cascadia margin, U.S.A. *Tectonics*, 9, 1-22.

621 Dawson, S., Smith, D.E., Ruffman, A., Shi, S. 1996. The diatom biostratigraphy of tsunami
622 sediments: Examples from recent and middle Holocene events. *Physics and Chemistry of*
623 *the Earth*, 21, 87-92

624 Demets, C., Gordon, R. G., Argus, D. F., Stein, S., 1990. Current plate motions. *Geophysical*
625 *Journal International*, 101, 425-478.

626 Dura, T., Rubin, C.M., Kelsey, H.M., Horton, B.P., Hawkes, A., Vane, C.H., Daryono, M., Grand
627 Pre, C., Ladinsky, T., Bradley, S. 2011. Stratigraphic record of Holocene coseismic
628 subsidence, Padang, West Sumatra. *Journal of Geophysical Research: Solid Earth* 116,
629 B11306.

630 Garrett, E., Shennan, I., Watcham, E.P., Woodroffe, S.A., 2013. Reconstructing paleoseismic
631 deformation, 1: modern analogues from the 1960 and 2010 Chilean great earthquakes.
632 *Quaternary Science Reviews*, 75, 11-21

633 Gehrels, W. R., Roe, H. M., Charman, D. J. 2001. Foraminifera, testate amoebae and diatoms
 634 as sea-level indicators in UK saltmarshes: a quantitative multiproxy approach. *Journal of*
 635 *Quaternary Science*, 16, 201-220.

636 Goldfinger, C.; Nelson, C.H., Morey, A., Johnson, J.E., Gutierrez-Pastor, J., Eriksson, A.T.,
 637 Karabanov, E., Patton, J., Gracia, E., Enkin, R., Dallimore, A., Dunhill, G., Vallier, T. 2012.
 638 Turbidite event history: Methods and implications for Holocene Paleoseismicity of the
 639 Cascadia Subduction Zone. United States Geological Survey Professional Paper 1661-F, 184
 640 pp.

641 Grand Pre, C. A., Horton, B.P., Kelsey, H. M., Rubin, C.M., Hawkes, A.D., Daryono, M.R.,
 642 Rosenberg, G., Culver, S.J. 2012. Stratigraphic evidence for an early Holocene earthquake
 643 in Aceh, Indonesia. *Quaternary Science Reviews*, 54, 142-151.

644 Hamilton, S., Shennan, I., 2005. Late Holocene relative sea-level changes and the earthquake
 645 deformation cycle around upper Cook Inlet, Alaska. *Quaternary Science Reviews*, 24, 1479-
 646 1498.

647 Hemphill-Haley, E., 1996. Diatoms as an aid in identifying late-Holocene tsunami deposits.
 648 *The Holocene*, 6, 439-448.

649 Hogg, A.G., Hua, Q., Blackwell, P.G., Niu, M., Buck, C.E., Guilderson, T.P., Heaton, T.J.,
 650 Palmer, J.G., Reimer, P.J., Reimer, R.W., Turney, C.S.M., Zimmerman, S.R.H., 2013. SHCal13
 651 Southern Hemisphere Calibration, 0-50,000 Years cal BP. *Radiocarbon*, 55(4).

652 Hua, Q., Barbetti, M., 2004. Review of tropospheric bomb C-14 data for carbon cycle
 653 modelling and age calibration purposes. *Radiocarbon*, 46, 1273-1298.

654 Jankaew, K., Atwater, B., Sawai, Y., Choowong, M., Charoentitirat, T., Martin, M.E.,
 655 Prendergast, A., 2008. Medieval forewarning of the 2004 Indian Ocean tsunami in Thailand.
 656 *Nature*, 405, 1228-1231.

657 Juggins, S. 2011. *C2 software package*. Newcastle University

658 Keys, J.G., 1963. The tsunami of 22 May 1960, in the Samoa and Cook Islands, *Bulletin of the*
 659 *Seismological Society of America*, 53, 1211-1227.

660 Lander, J. F., Lockridge, P. A., 1989, *United States tsunamis 1690-1988*. National Geophysical
 661 Data Center publication, v. 41-42.

662 Lomnitz, C. L., 1970. Major earthquakes and tsunamis in Chile during the period 1535 to
 663 1955. *Geologische Rundschau*, 59, 938-960.

664 Long, A.J., Shennan, I., 1994. Sea level changes in Washington and Oregon and the
 665 "Earthquake deformation cycle". *Journal of Coastal Research*, 10, 825-838.

666 Moernaut, J., Van Daele, M., Heirman, K., Fontijn, K., Strasser, M., Pino, M., Urruita, R., de
 667 Batist, M. 2014. Lacustrine turbidites as a tool for quantitative earthquake reconstruction:
 668 New evidence for a variable rupture mode in south central Chile. *Journal of Geophysical*
 669 *Research*, 119, 1607-1633.

670 Nelson, A. R., Shennan, I., Long, A. J., 1996. Identifying coseismic subsidence in tidal-wetland
 671 stratigraphic sequences at the Cascadia subduction zone of western North America.
 672 *Journal of Geophysical Research-Solid Earth*, 101, 6115-6135.

673 Nelson, A. R., Kashima, K., Bradley, L. A. 2009. Fragmentary Evidence of Great-Earthquake
 674 Subsidence during Holocene Emergence, Valdivia Estuary, South Central Chile. *Bulletin of*
 675 *the Seismological Society of America*, 99, 71-86.

676 Palmer, A.J.M., Abbott, W.H. 1986. *Diatoms as indicators of sea-level change*. In van de
 677 Plassche, O. (editor), *Sea-level research*. Free University, 457-87.

678 Patterson, R. T., Dalby, A. P., Roe, H. M., Guilbault, J. P., Hutchinson, I., Clague, J. J. 2005.
 679 Relative utility of foraminifera, diatoms and macrophytes as high resolution indicators of
 680 paleo-sea level in coastal British Columbia, Canada. *Quaternary Science Reviews*, 24, 2002-
 681 2014.

682 Peltier, W.R., 2004. Global glacial isostasy and the surface of the ice-age earth: The ICE-5G
 683 (VM2) model and GRACE. *Annual Review of Earth and Planetary Sciences*, 32, 111-149.

684 Plafker, G., Savage, J. C., 1970. Mechanisms of Chilean earthquakes of May 21 and May 22,
685 1960. *Geological Society of America Bulletin*, 81, 1001-1030.

686 Sawai, Y., Jankaew, K., Martin, M.E., Prendergast, A., Choowong, M., Charoentitirat, T. 2009.
687 Diatom assemblages in tsunami deposits associated with the 2004 Indian Ocean tsunami at
688 Phra Thong Island, Thailand. *Marine Micropaleontology*, 73, 70-79.

689 Sawai, Y., Namegaya, Y., Okamura, Y., Satake, K., Shishikura, M., 2012. Challenges of
690 anticipating the 2011 Tohoku earthquake and tsunami using coastal geology. *Geophysical*
691 *Research Letters* 39, L21309.

692 Sawai, Y., Nasu, H., Yasuda, Y. 2002. Fluctuations in relative sea-level during the past 3000 yr
693 in the Onnetoh estuary, Hokkaido, northern Japan. *Journal of Quaternary Science*, 17, 607-
694 622.

695 Sawai, Y., Satake, K., Kamataki, T., Nasu, H., Shishikura, M., Atwater, B., Horton, B.P., Kelsey,
696 H., Nagumo, T., Yamaguchi, M., 2004. Transient uplift after a 17th-century earthquake
697 along the Kuril subduction zone. *Science* 306, 1918–1920.

698 Shennan, I., Long, A.J., Rutherford, M.M., Green, F.M., Innes, J.B., Lloyd, J.M., Zong, Y.,
699 Walker, K.J., 1996. Tidal marsh stratigraphy, sea-level change and large earthquakes, I: A
700 5000 year record in Washington, USA. *Quaternary Science Reviews*, 15, 1023-1059.

701 Shennan, I., Scott, D. B., Rutherford, M., Zong, Y. Q. 1999. Microfossil analysis of sediments
702 representing the 1964 earthquake, exposed at Girdwood Flats, Alaska, USA. *Quaternary*
703 *International*, 60, 55-73.

704 Shennan, I., Barlow, N., Carver, G., Davies, F., Garrett, E., Hocking, E. 2014. Great
705 tsunamigenic earthquakes during the past 1000 yr on the Alaska megathrust. *Geology*, 42,
706 687-690.

707 Sieh, K., Natawidjaja, D.H., Meltzner, A.J., Shen, C.-C., Cheng, H., Li, K.-S., Suwargadi, B.W.,
708 Galetzka, J., Philibosian, B., Edwards R.L., 2008. Earthquake supercycles inferred from sea-
709 level changes recorded in the corals of west Sumatra. *Science* 322, 1674–1678.

710 St-Onge, G., Chapron, E., Mulsow, S., Salas, M., Viel, M., Debret, M., Debret, M., Foucher, A.,
711 Mulder, T., Winiarski, T., Desmet, M., Costa, P.J.M., Ghaleb, B., Jaouen, A., Locat, J. 2012.
712 Comparison of earthquake-triggered turbidites from the Saguenay (Eastern Canada) and
713 Reloncavi (Chilean margin) Fjords: Implications for paleoseismicity and
714 sedimentology. *Sedimentary Geology*, 243, 89-107.

715 Stein, S., Engeln, J. F., Demets, C., Gordon, R. G., Woods, D., Lundgren, P., Argus, D., Stein, C.,
716 Wiens, D. A. 1986. The Nazca-South America convergence rate and the recurrence of the
717 great 1960 Chilean earthquake. *Geophysical Research Letters*, 13, 713- 716.

718 Vita-Finzi, C. 2011. Misattributed tsunamis: Chile, Sumatra and the subduction model.
719 *Proceedings of the Geologists' Association* 122, 343-346.

720 Wang, P.-L., Engelhart, S. E., Wang, K., Hawkes, A. D., Horton, B. P., Nelson, A. R., Witter, R.
721 C., 2013. Heterogeneous rupture in the great Cascadia earthquake of 1700 inferred from
722 coastal subsidence estimates. *Journal of Geophysical Research: Solid Earth*,
723 doi:10.1002/jgrb.50101.

724 Witter, R. C., Kelsey, H. M., Hemphill-Haley, E. 2001, Pacific storms, El Nino and Tsunamis,
725 Competing mechanisms for sand deposition in a coastal marsh, Euchre Creek, Oregon,
726 *Journal of Coastal Research*, 17, 563-583.

727 Wright, C., Mella, A., 1963. Modifications to the soil pattern of south-central Chile resulting
728 from seismic and associated phenomena during the period May to August 1960.
729 *Seismological Society of America Bulletin*, 53, 1367-1402.

Figure captions

Figure 1: Tectonic setting of the Chilean subduction zone and the location of the field site. a. Spatial distribution of zones of uplift (blue ellipses; lighter shading where inferred) and subsidence (red ellipse) during the 1960 earthquake (following Plafker and Savage, 1970); b. Bahía Quetalmahue, northern Isla de Chiloé. Cisternas *et al.* (2005) studied the paleoseismic site at Rio Maullín; c. the coring transect across tidal and freshwater meadow at Chucalén, western Bahía Quetalmahue.

Figure 2: Schematic cross-section of a subduction zone showing vertical deformation during phases of interseismic strain accumulation (top) and coseismic strain release (bottom), modified from Hyndman and Wang (1993).

Figure 3: Stratigraphy of the coring transect at Chucalén, including a photograph of the sampled exposure with the four buried soils labelled A – D. Divisions on photograph scale bar = 10 cm. The exposure provides the sediments for diatom and radiocarbon analyses reported here.

Figure 4: *P-sequence* age-depth model for the Chucalén exposure, based on radiocarbon dates in Table 1. We calibrate post-bomb samples using the post-bomb atmospheric southern hemisphere ^{14}C curve (Hua and Barbetti, 2004) and enter them into OxCal v.4.2 (Bronk Ramsey, 2009) as *C_Dates* to make use of the unique solutions inferred from matching samples to the rising and falling limbs of the calibration curve (supplementary Figure S1). We calibrate pre-bomb samples using the SHCal13 calibration curve (Hogg *et al.*, 2013). We adjust the sample depths to exclude the sand layers overlying Soils A, B and D, which we interpret as tsunamis (discussed in section 5.1).

756

757 Figure 5: Summary of Chucalén diatom assemblages and relative sea-level reconstruction
758 derived from calibration of assemblages using the south central Chile transfer function
759 (Garrett *et al.*, 2013). Species classified as sub- or supra-MHHW based on modern species
760 elevation optima derived from the transfer function. We use the distance to the closest
761 modern analogue from the modern analogue technique in the C2 software package (Juggins,
762 2011) to assess the similarity between modern and fossil assemblages.

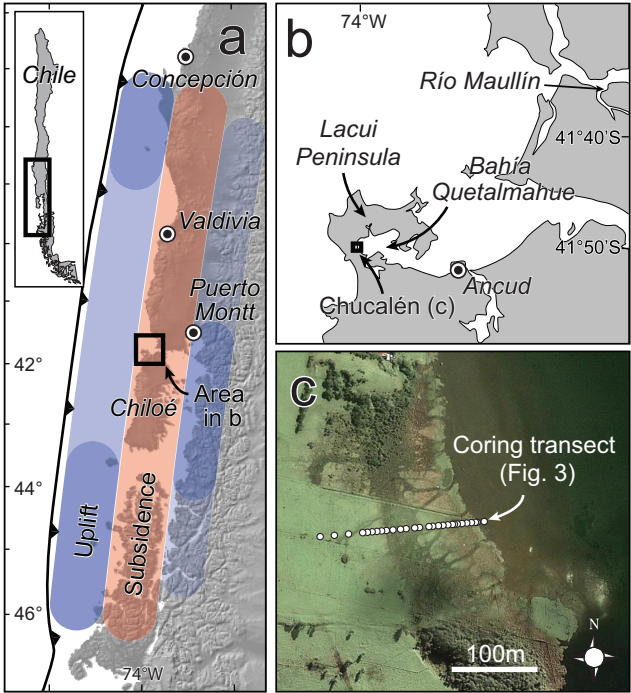
763

764 Figure 6: Comparison of the timing of earthquakes inferred from varve-dated turbidites from
765 three lakes to the north east of Valdivia (Moernaut *et al.*, 2014), pooled radiocarbon ages
766 primarily from plants killed by subsidence at Maullín (Cisternas *et al.*, 2005), *P_sequence*
767 modelling of radiocarbon dates at Chucalén (this study) and historically documented
768 earthquakes. Data from Chucalén and Maullín presented as calibrated radiocarbon date
769 probability distributions; Maullín data provide maximum ages for each earthquake; turbidite
770 ages expressed as median age from repeated varve counts (circles), with the error
771 (horizontal lines) being the difference between the median and outermost counts.
772 Additional lacustrine turbidites (ages not plotted) suggest further ruptures of smaller
773 coseismic slip and extent in AD 1466 ± 4 years, AD 1737 and AD 1837 (Moernaut *et al.*,
774 2014).

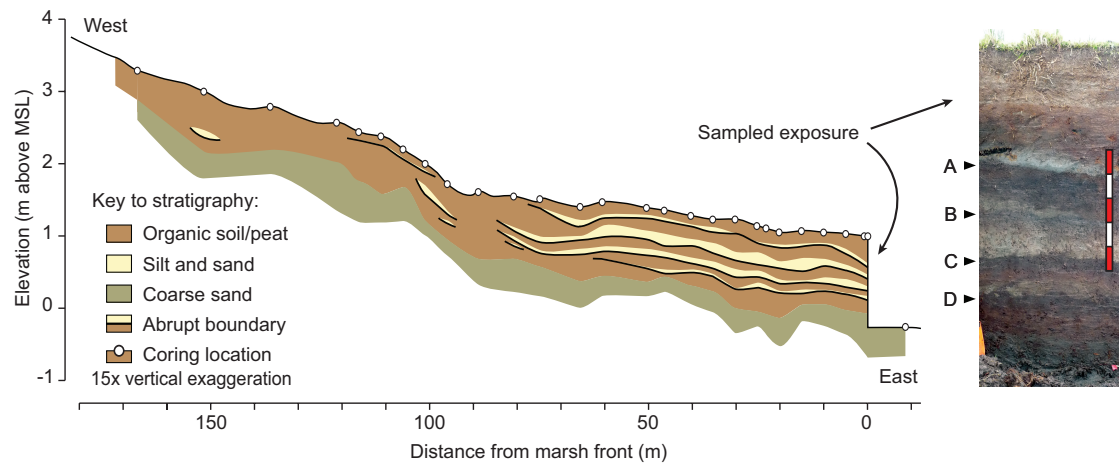
775

776 Figure 7: Relative sea-level change at Chucalén in a regional mid to late Holocene context.
777 This figure replicates the relative sea-level reconstructions in Figure 5, with the addition of
778 age ranges for each sample derived from the age model in Figure 4.

779



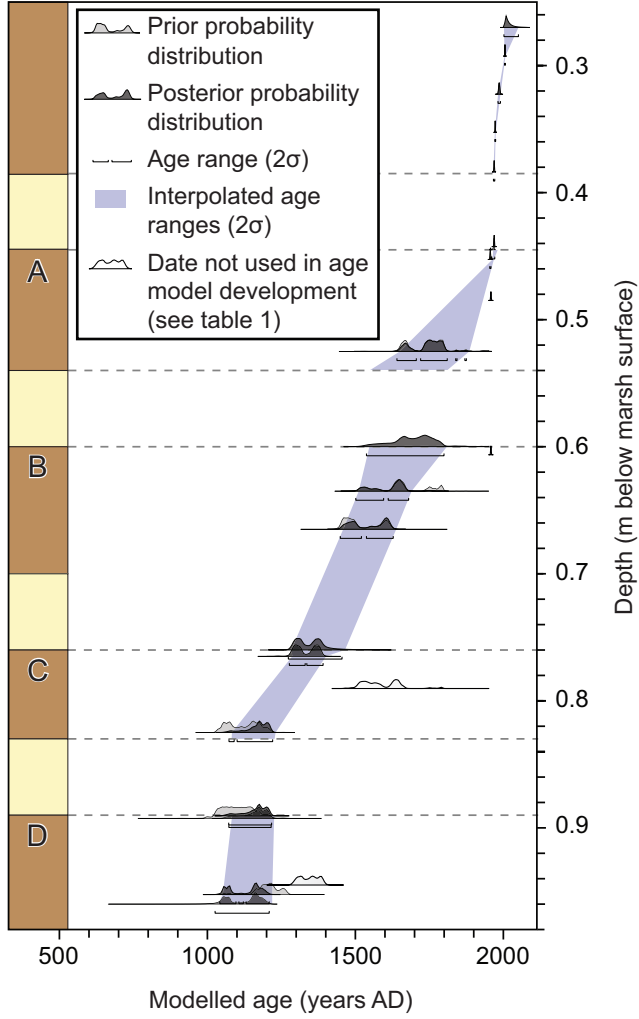
782



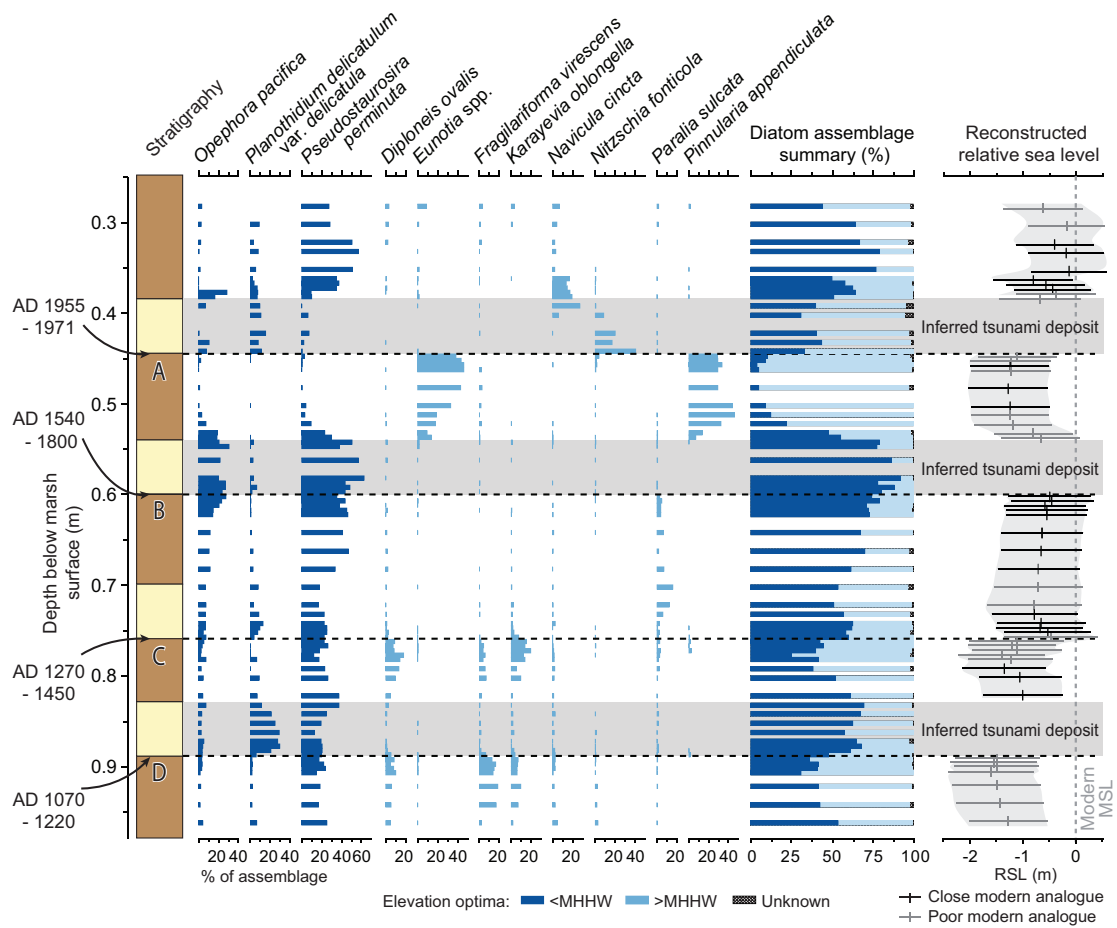
783

784

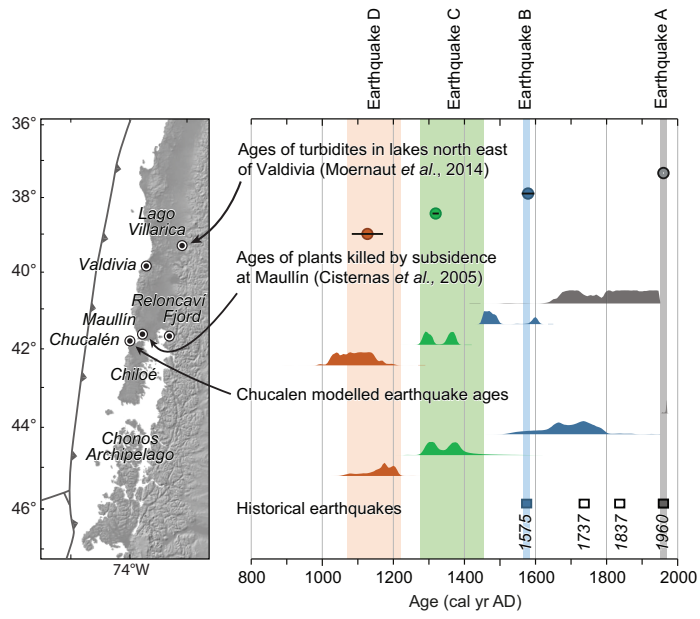
785



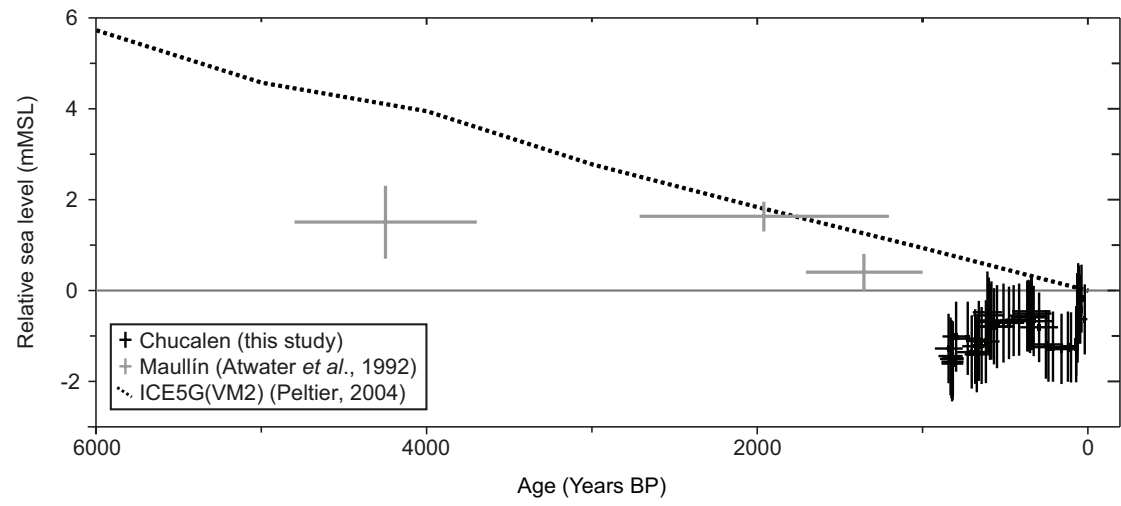
786



787
788



789
790



791
792

Laboratory code	Sample number	Central depth (cm)	Radiocarbon age (years BP $\pm 1\sigma$ / $F^{14}C \pm 1\sigma$)	Calibrated age range (2 σ years AD)	<i>P</i> _sequence modelled age (2 σ years AD)	Posterior probability of being an outlier	Agreement index
<i>Chucalén radiocarbon samples</i>							A_{overall} = 69.1
SUERC-39263	CH11/R1	29.25	1.0646 \pm 0.0065	2004-2006 ^a	2004-2006	0.01	86.7
SUERC-39264	CH11/R2	32.25	1.2056 \pm 0.0076	1982-1990 ^a	1982-1990	0.01	100.5
SUERC-39265	CH11/R3	35.25	1.4537 \pm 0.0092	1971-1973 ^a	1971-1974	0.04	86.8
SUERC-39266	CH11/R4	38.25	1.5337 \pm 0.0097	1967-1971 ^a	1966-1971	0.01	100.7
SUERC-39269	CH11/R5	45.25	1.0159 \pm 0.0064	1954-1958 ^a	1954-1958	0.14	99.7
SUERC-41189	CH11/R6	49.25	1.0964 \pm 0.0048	1956-1960 ^a	-	0.20	-
SUERC-41190	CH11/R7	52.5	234 \pm 35	1636-1950 ^b	1641-1875	0.21	104
SUERC-43050	CH11/R8	60.5	1.1042 \pm 0.0052	1956-1960 ^a	-	0.85	-
SUERC-43051	CH11/R9	63.5	285 \pm 38	1505-1800 ^b	1501-1680	0.04	112.6
SUERC-43052	CH11/R10	66.5	427 \pm 38	1441-1626 ^b	1449-1628	0.04	90.9
SUERC-41191	CH11/R11	76.5	713 \pm 35	1278-1391 ^b	1277-1391	0.07	98.9
SUERC-43048	CH11/R12	79.5	317 \pm 38	1487-1794 ^b	-	0.98	-
SUERC-41187	CH11/R13	82.5	950 \pm 35	1037-1209 ^b	1072-1221	0.34	89.6
SUERC-39270	CH11/R14	89.25	979 \pm 51	1020-1210 ^b	1072-1216	0.15	76.7
SUERC-40031	CH11/R15	92.25	680 \pm 37	1290-1396 ^b	-	0.90	-
SUERC-40032	CH11/R16	95.25	881 \pm 37	1070-1275 ^b	1042-1210	0.09	50.6

794 ^a Calibrated using the post-bomb atmospheric southern hemisphere ¹⁴C curve (Hua and Barbetti,

795 2004)

796 ^b Calibrated using SHCal13 (Hogg *et al.*, 2013)

797

798 Table 1: Calibrated radiocarbon dates from plant macrofossils from the Chucalén exposure.

799 Dates modelled in a *P*_sequence deposition model in OxCal 4.2 (Bronk Ramsey, 2009), with a

800 k value of 50. Outlier analysis provides the posterior probability of each sample being an

801 outlier; prior probabilities set to 0.05; posterior probabilities exceeding 0.4 considered to be

802 significant outliers. The age of samples CH11/R6, CH11/R8, CH11/R12 and CH11/R15 do not

803 fit in with the stratigraphic sequence and are not used in age model development.

Earthquake associated with burial of Soil	Magnitude of coseismic deformation (m \pm 2 σ)
A	-1.12 \pm 1.04
B	0.08 \pm 1.07
C	-0.92 \pm 1.20
D	-0.60 \pm 1.10

804

805 Table 2: Vertical coseismic deformation estimates for the four earthquakes obtained by
806 calibrating Chucalén diatom assemblages with the south central Chile transfer function
807 model (Garrett *et al.*, 2013). Uplift is positive, subsidence is negative. Estimates are
808 corrected for sedimentation.

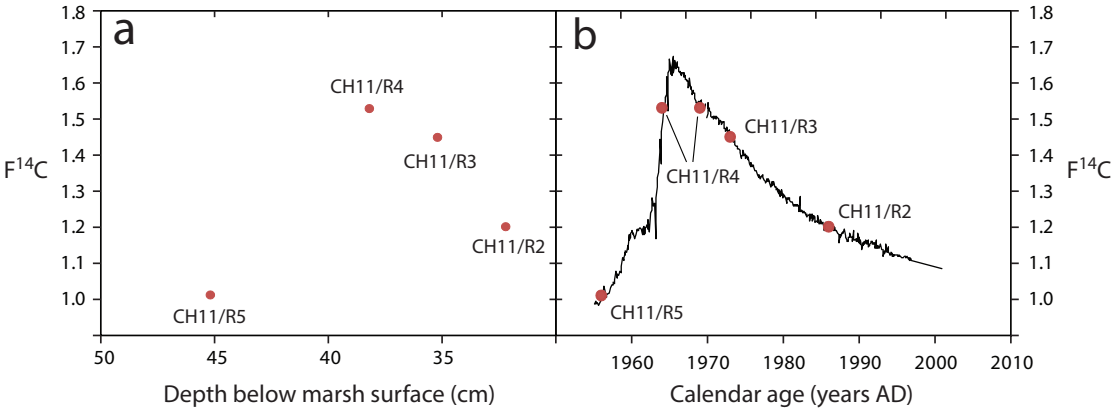


Figure S1: Chucalén bomb spike samples, a. plotted as $F^{14}C$ against depth below the marsh surface and b. fitted to the post-bomb atmospheric southern hemisphere ^{14}C curve (black line) of Hua and Barbetti (2004). Sample CH11/R5 must lie on the rising limb, sample CH11/R4 may lie on either the rising or the falling limb and samples CH11/R3 and CH11/R2 must lie on the falling limb.

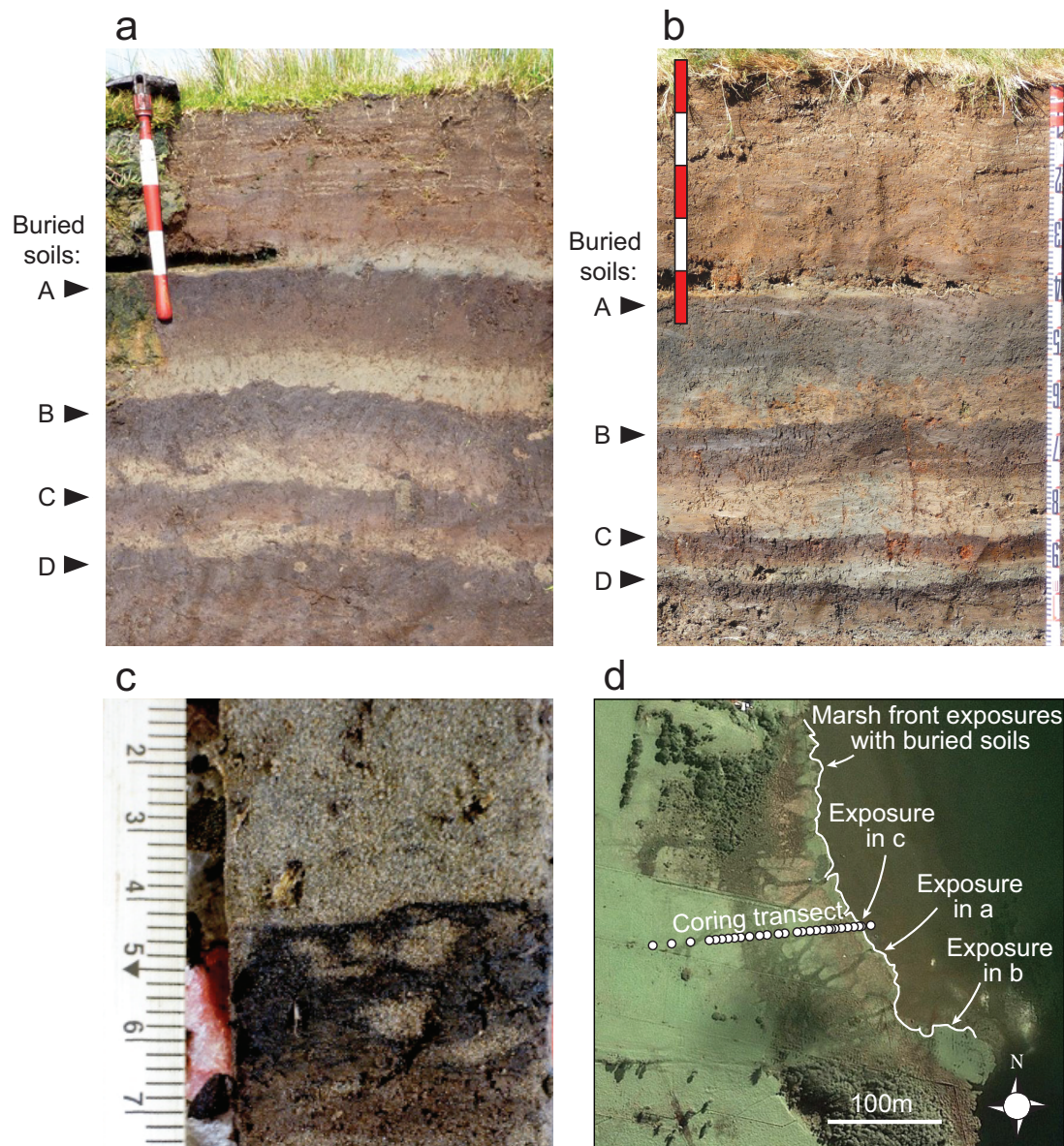


Figure S2: Photographs of Chucalén marsh front exposures. a. and b. display the four buried soils, labelled A-D, in exposures south east of the coring transect. Divisions on scale bars = 10 cm. c. The upper contact of Soil C, displaying burrows filled with the overlying silty sand. d. Map showing the extent of marsh front exposures with visible buried soils, the locations of photographed exposures and the coring transect illustrated in Figure 3.